METHODS PAPER

Cartesian coordinates in two-dimensional bone histology images ~~are useful~~ in Quaternary bone remodelling research

Justyna J. Miszkiewicz[1,2,3], Julien Louys[4], Patrick Mahoney[3]

[1]School of Archaeology and Anthropology, Australian National University, Canberra, Australia

[2]School of Social Science, University of Queensland, Brisbane, Australia

[3]Skeletal Biology Research Centre, University of Kent, Canterbury, United Kingdom

[4]Australian Research Centre for Human Evolution, Griffith University, Brisbane, Australia

ABSTRACT

Palaeohistologists who work with well-preserved hominin cortical bone can examine two-dimensional (2D) histology images for quantitative parameters of secondary osteons and Haversian canals to reconstruct past bone remodelling. Standard techniques in this space ~~have~~ included ~~taking~~ area measurements and counts of histology components recorded from an ~~seen in an~~ image. The 'point-count' technique involves counting all the items (e.g., secondary osteons, osteocyte lacunae) of interest per image area. The open access image analysis software ImageJ/ FIJI facilitates this technique in a user-friendly way. Raw data points are captured and can be saved in a spreadsheet. Aside from the total number of counts, the software also issues Cartesian (XY) coordinates locating each counted point. These XY coordinates are typically neglected within palaeohistological approaches due their assumed irrelevance to research questions of bone remodelling significance. We provide a short evaluation of XY coordinates captured by ImageJ/FIJI from 2D bone histology images, and a protocol for a simple calculation of XY distances that follow the path of point counting. We focus on osteocyte lacunae which serve as a proxy for osteoblast-osteocyte conversion in live bone by replicating the protocol on a bone sample from a Medieval English individual. We discuss the potential of XY coordinates for reconstructing the proximity of ~~efficient representation of how closely situated the counted~~ osteocyte lacunae~~/points are,~~ and related ~~thus indicating localised~~ bone remodelling activity through exchange of nutrients by neighbouring cells. We recommend palaeohistologists report XY coordinate data in their results to ensure better hominin palaeobiology characterisation.

Keywords: hominins; image analysis; histomorphometry; bone remodelling; ImageJ

1. INTRODUCTION

Quantitative analysis of histology images (histomorphometry) is a gold standard in various biological disciplines that collect data about tissue cells and other microscopic structures (e.g., Erben & Glösmann 2019; Revell 1983; O'Driscoll et al. 1999; Villa & Lynnerup 2010). Histology can also be applied to bones that derive from palaeontological and archaeological contexts to reconstruct remodelling processes that occur throughout an animal's lifespan and respond to internal and environmental stimuli (e.g., Bromage et al. 2009; Cook et al. 1998; Crowder & Stout 2011; de Buffrénil et al. 2021; Miszkiewicz 2015; Sawada et al. 2004; Stout & Stanley 1991). One useful analytical approach in bone histology ~~examination~~ is quantifying geometric and density properties of secondary/ Haversian bone tissue seen microscopically in thin sections taken in a transverse plane (Stout & Crowder 2012) (Figure 1). The histological appearance of Haversian bone reflects the activity of Bone Multicellular Units (BMUs) which are three-dimensional (3D) cell structures that execute bone remodelling in live bone by 'digging' longitudinal tunnels as bone is resorbed and deposited (Figure 2) (Lassen et al. 2017; Maggiano et al. 2016; Sims & Martin 2014). Once quantified, cortical bone histology data can be studied at an individual or large sample level representing past populations (e.g., Chan, Crowder & Rogers 2007; Stout & Lueck 1995; Miszkiewicz et al. 2020).

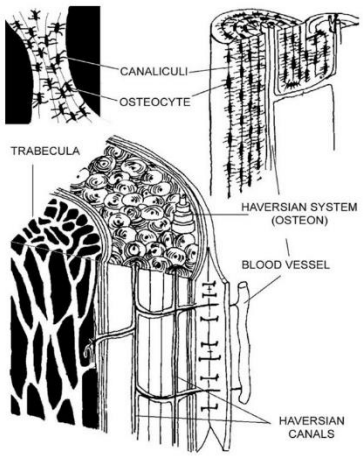

Figure 1. Sketch of the microscopic components of bone showing Haversian systems and osteocytes. Reproduced from Smit et al. 2002 p. 2022, with permissions from John Wiley and Sons under licence 5297961008734.

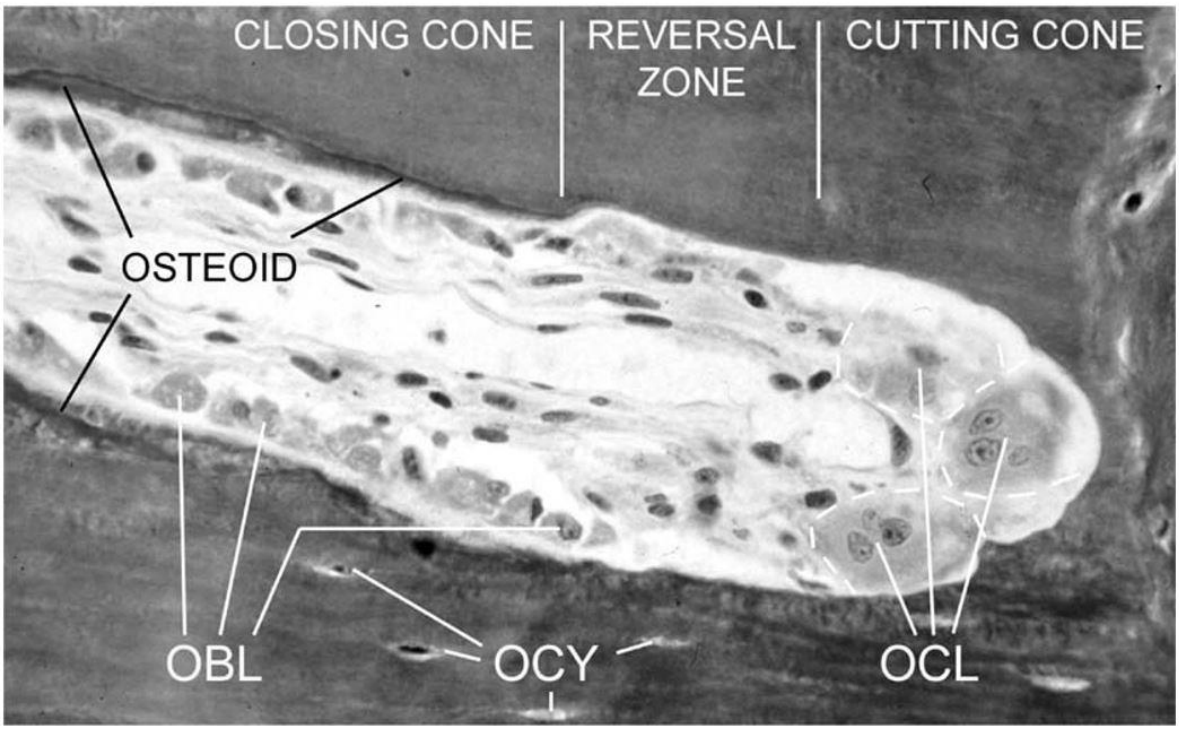

Figure 2. An example of an active Bone Multicellular Unit (BMU) showing osteoclasts (OCL), osteoblasts (OBL), and osteocytes (OCY). Image is not to scale, but the width of the BMU would be approximately 200 μm. Reproduced from Smit et al. 2002 p. 2024, with permissions from John Wiley and Sons under licence 5297961008734.

All bone biologists who undertake histomorphometry are expected to follow recommended guidelines for unified nomenclature and techniques used in calculating parameters of bone remodelling (Dempster et al. 2013). Working with Haversian tissue, the relevant quantifiable histology variables include the area, diameter, density, and circumference of structures such as secondary osteons, Haversian canals, and osteocyte(s)/lacunae (osteocytes do not always preserve in post-mortem bone, so osteocyte lacunae indicate where the osteocytes had resided) (Crowder & Stout 2012; Hunter & Agnew 2016; Stout, Cole & Agnew, 2019; Bromage et al. 2009). The densities of secondary osteons or osteocyte lacunae are typically calculated by summing up the total counts seen in a specified field of view or a selected region of interest (ROI), and then dividing the raw count by the area examined (Crowder & Stout 2012; Crowder et al. 2022; Drew, Mahoney & Miszkiewicz 2021). This counting approach is known as the 'point count' technique (Stout & Stanley 1991). Secondary osteon density, referred to as osteon population density (OPD), data reflect the amount of remodelled bone per area (Frost 1987), whereas osteocyte density reflects osteoblast-osteocyte conversion (Bromage et al. 2016).

While these densities have been reported by multiple studies investigating topics that have ranged from biomechanics (Drew, Mahoney & Miszkiewicz, 2021), diet (Paine & Brenton 2006), to human evolution (Sawada et al. 2004), a notable gap in analyses is that the proximities of individual counted points are not considered. This is interesting because biologists regularly consider dispersal or proximity analysis when analysing points against a specified area to assess the randomness, clustering, or migration of cells (Cruz et al. 2005; Fernández, Lysakowski & Goldberg, 1995; Gorelik & Gautreau 2014; Wang et al. 2021). Only a handful of palaeontological, bioarchaeology, or anthropological studies haves considered spatial distribution relationships within bone histology sections. This has included Rose et al. (2012), and Gocha and Agnew (2016), who brought to light the value of applying Geographic Information Systems (GIS) software in understanding osteon population dispersal across complete human metatarsal and femoral bone cross-section shafts, respectively. Further, Miszkiewicz et al. (2020) applied GIS to measure distances between neighbouring Haversian canals across thin sections from the femoral midshaft in an archaeological specimen, spatially mapping cortical bone porosity. GIS can require substantial training. An alternative, commonly used, user friendly, and self-intuitive, image analysis software is the open access ImageJ, part of the FIJI package (Schindelin et al. 2015). In this paper, we highlight that ImageJ/FIJI also registers XY coordinates alongside point counts and can be used to efficiently calculate path distances between neighbouring histology structures. We focus on hypothetical osteocyte lacunae in a sketched diagram, supply a manual protocol based on established mathematics for the path distance calculations, and then replicate it on a secondary osteon image from an archaeological (dated to Medieval England) human femur.

2. METHODS: XY COORDINATES IN IMAGEJ/FIJI

2.1. The protocol and application to a hypothetical sample

ImageJ/FIJI can be freely downloaded from the dedicated website (https://imagej.net/software/fiji/). The preparation of bone histology slides will not be covered here. A ready image with a known scale captured using a dedicated microscope camera is needed to apply the protocol we discuss. We note ImageJ/FIJI provides macros and plug-ins that calculate various other aspects of XY coordinates (e.g., distance from centroid), but these require coding and script amendments. Distances between selected

points can also be measured manually one by one using the "Straight line" tool of ImageJ/FIJI, but this approach takes more time than the presented XY coordinate analysis and has to be conducted in addition to point counting. We provide a manual guide for path distance calculations from the XY coordinate data recorded at the same time as point counts which is straightforward and efficient in its application.

The first step (Figure 3a) is to open ImageJ/FIJI (we used vol. 153o), import the image of interest, and set the appropriate scale ("Analyze" > "Set scale"). The counts of the osteocyte lacunae can be completed using the "Multi-point" function selected form the ImageJ/FIJI toolbar. For the distances to be most meaningful biologically, the sequence of counts made would ideally be either conducted starting at the Haversian canal and continuing outwards (towards the cement line), or *vice versa* (Figure 3b). That is because canaliculi, which connect successive osteocytes within a secondary osteon, are largely arranged radially so as to maximise fluid flow (van Tol et al. 2020). By pressing "M", the measurements can be obtained. A "Results" window will appear where the following measurements are recorded: "Area", "Mean", "Min", "Max", "X", "Y" (Figure 3c). The "X" and "Y" are the coordinate values that can be used to understand the proximity of these points. The output from the "Results" window can be saved as an Excel spreadsheet, or the XY coordinates can be copied and pasted into a new spreadsheet.

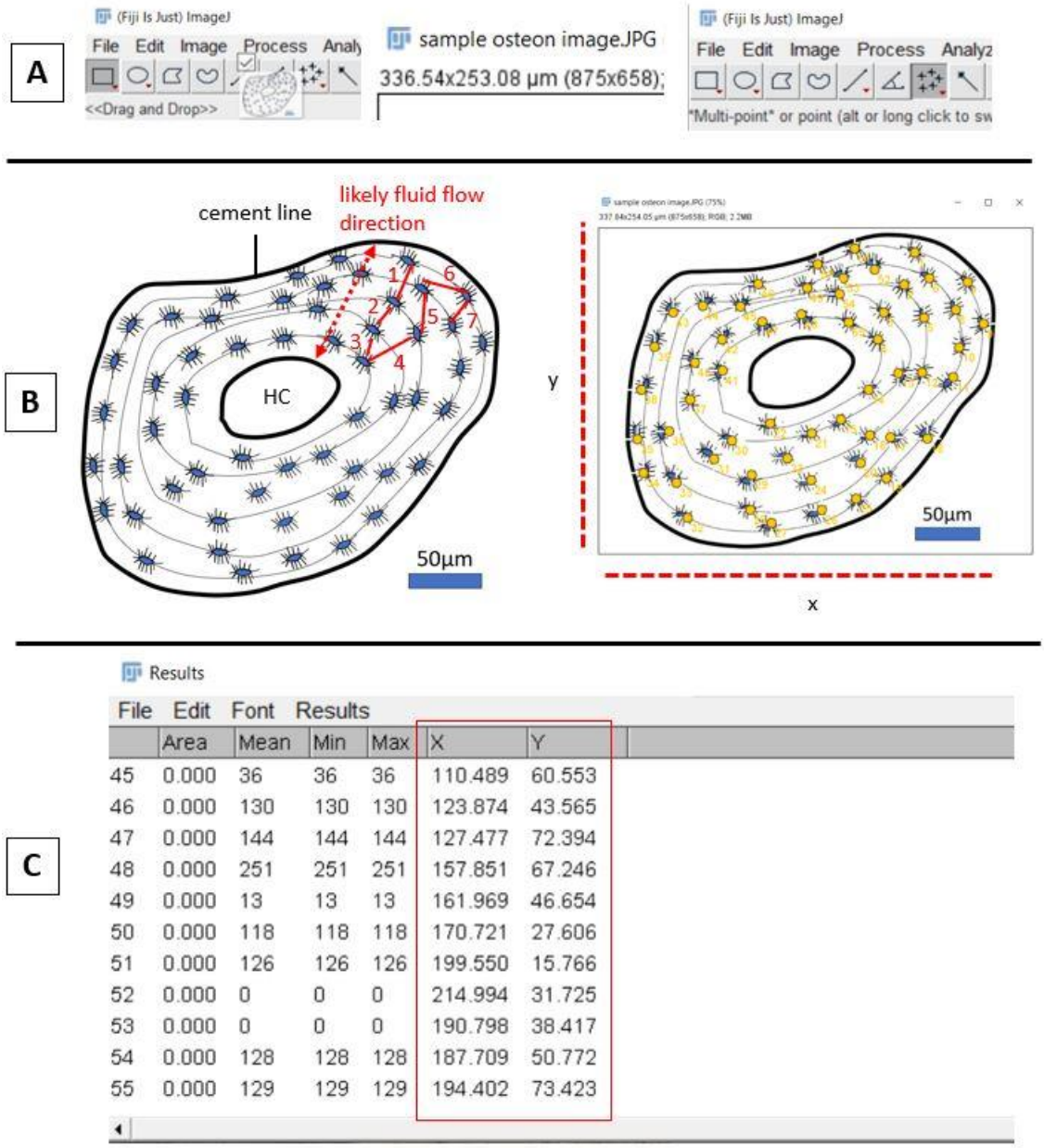

	Area	Mean	Min	Max	X	Y
45	0.000	36	36	36	110.489	60.553
46	0.000	130	130	130	123.874	43.565
47	0.000	144	144	144	127.477	72.394
48	0.000	251	251	251	157.851	67.246
49	0.000	13	13	13	161.969	46.654
50	0.000	118	118	118	170.721	27.606
51	0.000	126	126	126	199.550	15.766
52	0.000	0	0	0	214.994	31.725
53	0.000	0	0	0	190.798	38.417
54	0.000	128	128	128	187.709	50.772
55	0.000	129	129	129	194.402	73.423

Figure 3. Series of initial steps of point counting in ImageJ/FIJI. A: importing of image (HC: Haversian canal), setting the scale, and selecting the "Multi-Point tool". B: outline of secondary osteon diagram with osteocyte lacunae prior to (left), and after (right), counting of the lacunae. C: ImageJ/FIJI data window showing XY coordinates for each point (red box, left), transported into a spreadsheet (right).

The next step is to calculate the 2D distance between XY coordinates, following the path of counting, using the formula

$$D = \sqrt{(x_2 - x_1)^2 + (y_2 - y_1)^2}$$

(derived from the Pythagorean theorem) (Figure 4).

1. In the same or a new spreadsheet, new columns aligned next to each other can be created and named: X_{diff} (this will be the difference between successive X coordinates), Y_{diff} (this will be the difference between successive Y coordinates), D^2 (squared distance between X_{diff} and Y_{diff}), D (square root of D^2).
2. The difference between successive X and successive Y coordinates is then calculated individually (i.e., per axis). This can be achieved in Microsoft Excel by typing in "=cell with raw X value-preceding cell with raw X value" - the example in Figure 4 would be "=A3-A2". This then can be repeated on the Y coordinates. The last cell should not be considered because it does not have a successive coordinate. The cell function can be dragged down the entire column.
3. D^2, defined through the formula: $D^2 = X_{diff}^2 + Y_{diff}^2$, is then calculated. This can be achieved in Excel by typing "=cell with X_{diff}^2+cell with Y_{iff}^2". The example shown in Figure 4 would be "=C2^2+D2^2". The cell function can be dragged down the entire column.
4. Finally, the square root of D^2 is calculated which can be done in Excel by typing "=SQRT(cell with D^2 value). In Figure 4, the example would be "=SQRT(E2)". The cell function can be dragged down the entire column.

Raw data resulting from this hypothetical image analysis can be found in our Supplemental File. The resulting D values are the distances in the unit appropriate to the image between the XY coordinates registered along the pathway of counting. They can be analysed across a whole osteon, summarised as averages per osteon, a full image, individual, larger sample – whatever the desired level of analysis as per one's research question. In the presented example, the average distance across this one hypothetical secondary osteon was 28.25 μm (see Supplemental File).

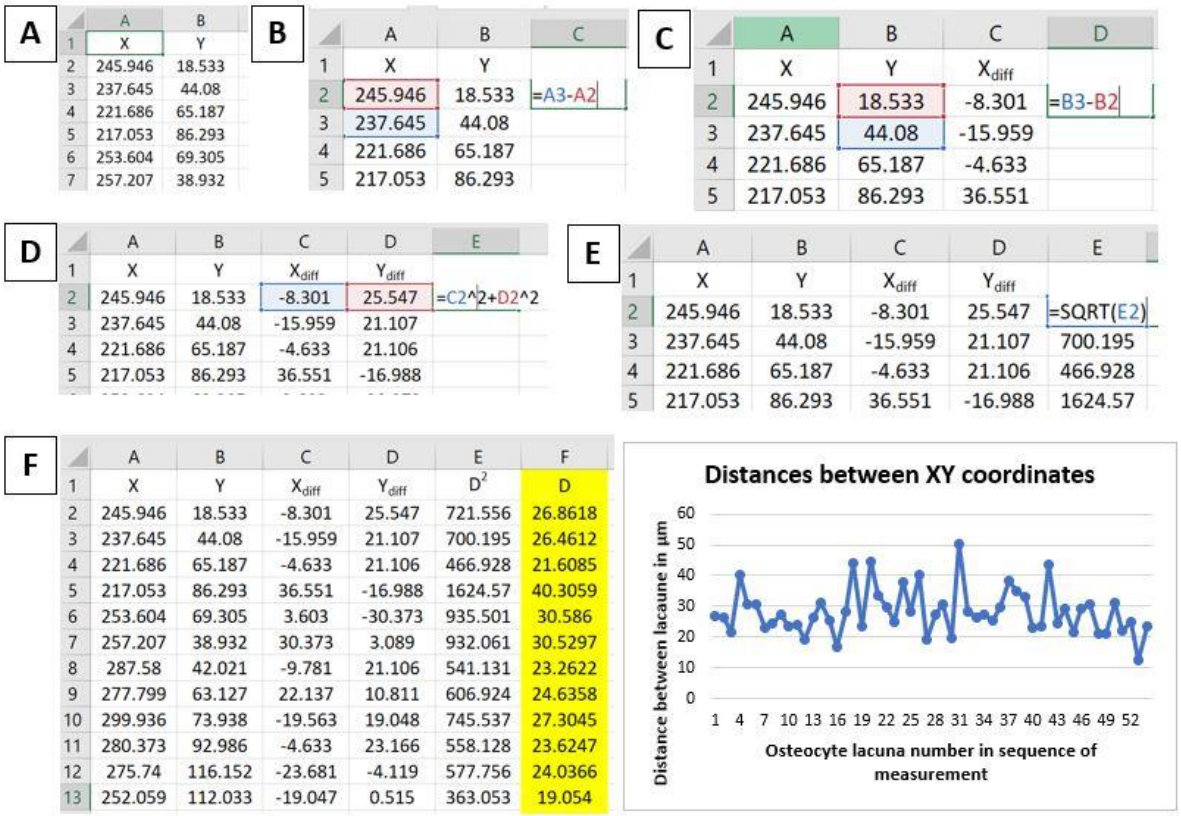

Figure 4. Screenshots of successive steps in XY distance coordinate calculations in Microsoft Excel. A: XY coordinates from the ImageJ/FIJI results output, B-C: calculating differences between successive X and Y coordinates, D: calculating the squared distance (D^2) between XY differences, E: calculating the square root of D^2, F: final distance values of XY coordinates (D) in µm (highlighted in yellow), which can be quickly visualised using a simple line graph.

2.2. Replication on an authentic sample

To validate this short protocol, we applied it step-by-step to a real case – using a cortical bone histology image showing a well-preserved secondary osteon in the femur of a Medieval English individual (ID: NGB89SK2). The thin section is a 100-µm thick slice of midshaft cortex extracted from the anterior aspect of the femur. This individual was estimated to be a middle-aged (35-50 years old) male (Miszkiewicz, 2014), and the sample is part of a larger collection of thin sections representing a Medieval English human osteological assemblage curated at the University of Kent, UK. These thin sections had been prepared following standard histology methods applied to archaeological human remains (Miszkiewicz, 2014). A full ethics board review was not required as this is an archaeological collection, but a local (School of Anthropology and Conservation) ethics application form and check list was filed on 11 November 2010 and approved by the 2010 Ethics Advisory Group at the University

of Kent, UK. In addition to curatorial permissions, all analyses on these sections follow codes of ethics and good practice as stipulated by the international biological anthropology bodies (British Association for Biological Anthropology and Osteoarchaeology; American Association of Biological Anthropologists). The anterior femur sample presented here was also previously included in research by Drew, Mahoney and Miszkiewicz et al. (2021), Miszkiewicz and Mahoney (2012), and Miszkiewicz (2014). The XY coordinate distance data are calculated here for the first time.

Using an Olympus BX60 high powered microscope equipped with a MIchrome 5 Pro SS-936 camera and operated using Capture v2.1 software, one secondary osteon showing clear cement lines (Figure 5A) and well-preserved osteocyte lacunae (Figure 5B) was selected from intra-cortical bone. It was viewed under linearly polarised light to check good preservation, i.e., ensuring that individual concentric lamellar rings could be seen clearly (Figure 5CD).

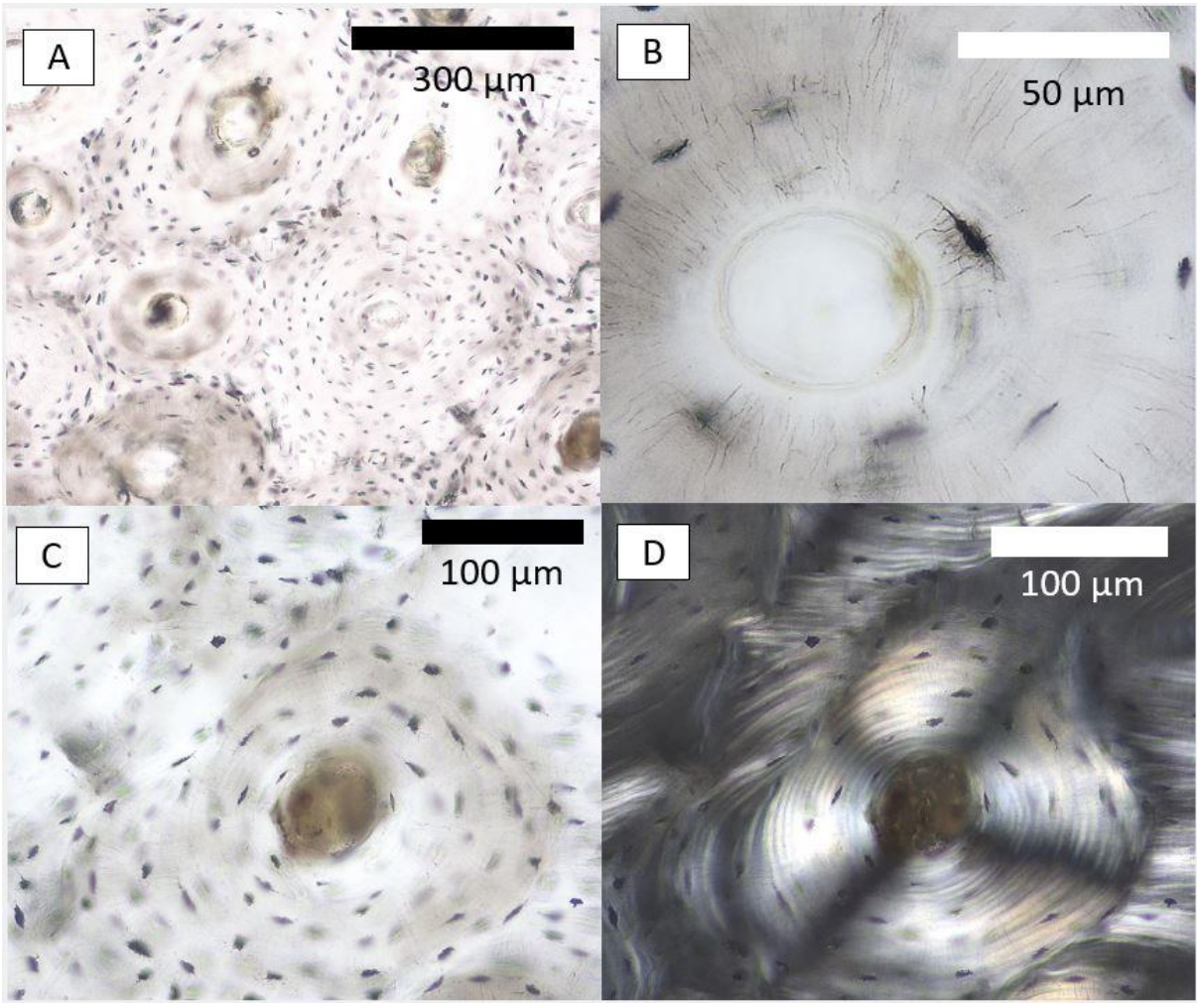

Figure 5. Cortical bone histology images in a sample from a Medieval English male (ID: NGB89SK2, St. Gregory's Priory and Cemetery collection, University of Kent, UK) taken from the anterior midshaft. Image A shows a cluster of secondary osteons with a range of osteocyte lacunae preservation. Image B shows a closeup of an osteocyte lacuna as an example of good preservation in the secondary osteon selected for our replication analysis. Images C and D show the secondary osteon under polarised transmitted (C) and linearly polarised light (D).

The secondary osteon image captured using transmitted light (so that each osteocyte lacuna could be identified easily (black lacunae against white bone)) was examined following our protocol above. The image was imported into ImageJ/FIJI (vol. 153o). Osteocyte lacunae were counted starting at the cement line and continuing towards the Haversian canal in a linear fashion (Figure 6). The resulting XY coordinates were used for calculating distances between the neighbouring osteocyte lacuna, the average of which for the entire secondary osteon was 24.84 μm.

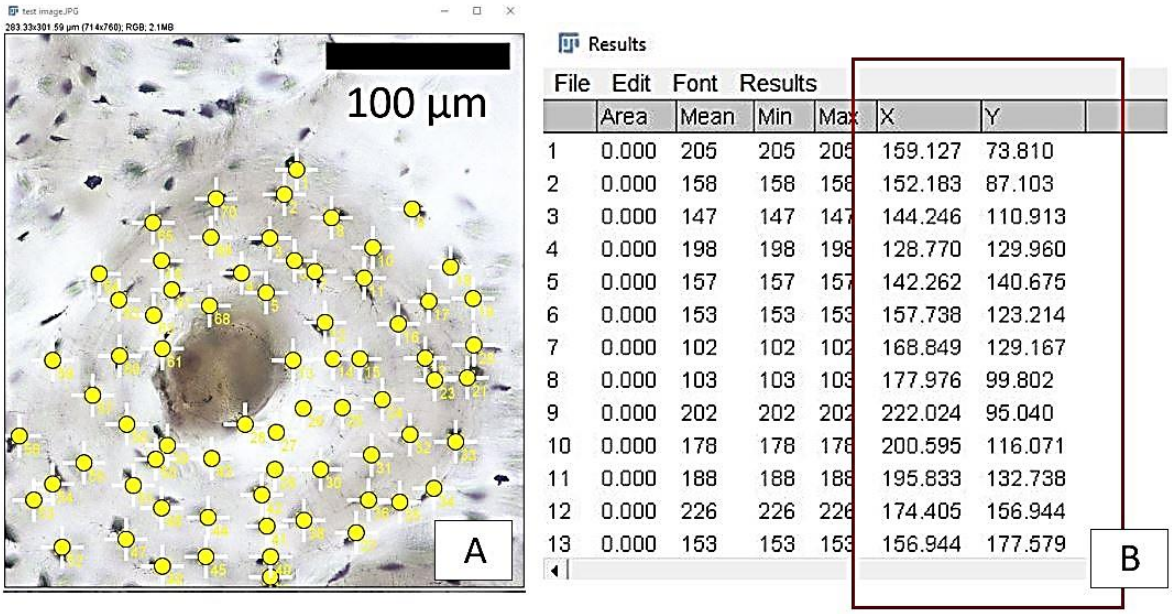

Figure 6. Screenshots of image analysis steps replicating our XY coordinate calculation protocol. A: secondary osteon with osteocyte lacunae (yellow dots). B: raw data output window in ImageJ/FIJI showing resulting XY coordinates (red rectangle).

	A	B	C	D	E	F
1	X	Y	X_{diff}	Y_{diff}	D^2	D
2	159.127	73.81	-6.944	13.293	224.923	14.99743
3	152.183	87.103	-7.937	23.81	629.9121	25.09805
4	144.246	110.913	-15.476	19.047	602.2948	24.54169
5	128.77	129.96	13.492	10.715	296.8453	17.2292
6	142.262	140.675	15.476	-17.461	544.3931	23.33223
7	157.738	123.214	11.111	5.953	158.8925	12.60526
8	168.849	129.167	9.127	-29.365	945.6054	30.7507
9	177.976	99.802	44.048	-4.762	1962.903	44.30466
10	222.024	95.04	-21.429	21.031	901.505	30.02507
11	200.595	116.071	-4.762	16.667	300.4655	17.33394
12	195.833	132.738	-21.428	24.206	1045.09	32.32785
13	174.405	156.944	-17.461	20.635	730.6897	27.03127
14	156.944	177.579	21.826	-0.793	477.0031	21.8404
15	178.77	176.786	14.682	0	215.5611	14.682
16	193.452	176.786	21.032	-19.048	805.1713	28.37554
17	214.484	157.738	16.667	-12.301	429.1035	20.71481
18	231.151	145.437	11.905	-18.651	489.5888	22.12665
19	243.056	126.786	12.301	17.063	442.4606	21.03475
20	255.357	143.849	0.397	25.397	645.1652	25.4001
21	255.754	169.246	-3.571	17.857	331.6245	18.21056

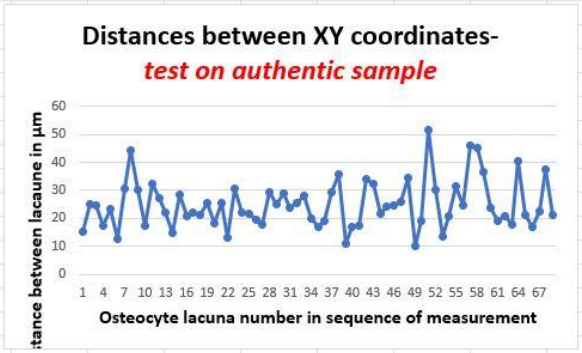

Figure 7. Screenshot of final calculations of distances between XY coordinates yielded using the Medieval English histology sample. Column F, highlighted in yellow, shows the D values in µm. The line graph illustrates variation in D values from across the entire secondary osteon.

3. DISUSSION: INTERPRETATIVE VALUE

We present here a simple and effective way to obtain an insight into the distances between neighbouring points ~~along a path of counting~~ in a 2D histology image. Those who regularly work with osteocyte lacunae or OPD data might already have raw data files from ImageJ/FIJI stored where the XY coordinates are saved. Certainly, whenever possible these should be provided alongside other commonly reported variables, either in the main body of an article or the online supplementary information. Re-analyses of data as outlined here may provide new insights into new or old research questions, although it is also vital to provide the sequence in which the points are counted. For example, very wide distances between some coordinates may simply reflect random and widespread counting across an image and thus have no meaning for understanding distances between neighbouring bone histology elements.

The interpretative value of the distances between osteocyte lacunae on a path of counting is that it would inform how well inter-connected osteocytes were in a given sample. This provides information about bone remodelling processes and how actively bone was maintained (Andreaus, Colloca & Iacoviello 2014; Bromage et al. 2009). This is because the inter-connectedness of neighbouring lacunae facilitates

healthy exchange of nutrients, bone biological signals, and fluid flow (Kollmannsberger et al. 2017; van Tol et al. 2020). For example, it has been suggested that, in humans, osteocyte-to-osteocyte distance of 20-30 μm is enough to facilitate effective dissemination of molecules (Chen et al. 2018; Wang et al. Sugawara et al. 2005). In our Medieval example, the resulting D values fell into this distance range, which could be used to infer that osteocyte communication was not disrupted in this region of bone. Canè et al. (2000) noted changes in osteocyte distribution depending on the long bone region (e.g., cortical vs trabecular bone, diaphysis vs metaphysis vs epiphysis). Thus, future research into osteocyte lacunae distance data applied across hominin bone could be placed within the wider bone biology knowledge and help further refine interpretations made from bone histology density and other geometric variables alone.

The XY coordinate distance measurements may not be as useful in understanding secondary osteon distribution as they might be when applied to osteocyte lacunae, simply because osteons can remodel both stochastically and in a targeted fashion (Martin 2007), so it is almost impossible to determine the timing (sequence of secondary osteon appearance) of remodelling from post-mortem, archaeological, or fossilised bone samples. Identifying the timing of remodelling would also be difficult to achieve when dealing with bone from older individuals that show several generations of remodelled secondary osteons, possibly reflecting an OPD asymptote (Frost 1987). However, the technique could be applicable to counts of intact osteons (see Crowder et al. 2022) across a relatively larger image area (or a shaft cross-section) to determine whether BMU products were operating in a clustered or dispersed manner, alongside the osteon density data.

The key limitation of using the XY coordinate distance in bone histology examination is, of course, the 2D level of perspective which does not capture the 3D nature of osteocytes or osteonal structures in a bone sample (Andronowski & Cole 2021). Another limitation is that the outlined calculations need to be processed manually, in the sense that they have to be analysed outside of ImageJ/FIJI. However, once the main cell functions are set up, the XY coordinates from the ImageJ/FIJI output can be simply copied and pasted into a spreadsheet (a template is supplied in our Supplemental File). The advantage of using ImageJ/FIJI lies in having access to a forum of supporting scholars who are continually

developing macros and plug-ins, and assist with coding, that can be used to calculate other XY coordinate distances that might be of interest to palaeohistologists (e.g. distance from centroid). Our protocol does not require significant training or access to expensive software and so would be applicable across a wide range of institutions, particularly where there is limited infrastructure (see Miszkiewicz 2020). While other disciplines can employ automated approaches to cell counting and measuring from 2D or 3D images (e.g., O'Driscoll et al. 1999), histologists working with archaeological or fossilised samples are hindered by issues with preservation, meaning that careful manual approaches to histology image analysis will continue to be needed. Being able to conduct manual XY coordinate counts could be a useful addition to the technical toolkit.

Acknowledgements

Miszkiewicz thanks the Australian Research Council for funding (DE190100068).

Competing interests

We have no competing interests to declare.

REFERENCES

Andreaus, U., Colloca, M., & Iacoviello, D. (2014). Optimal bone density distributions: numerical analysis of the osteocyte spatial influence in bone remodeling. *Computer Methods and Programs in Biomedicine*, 113(1), 80-91. https://doi.org/10.1016/j.cmpb.2013.09.002

Andronowski, J. M., & Cole, M. E. (2021). Current and emerging histomorphometric and imaging techniques for assessing age-at-death and cortical bone quality. *Forensic Science*, 3(2), e1399. https://doi.org/10.1002/wfs2.1399

Bromage, T.G., Lacruz, R.S., Hogg, R., Goldman, H.M., McFarlin, S.C., Warshaw, J., Dirks, W., Perez-Ochoa, A., Smolyar, I., Enlow, D.H., & Boyde, A. (2009). Lamellar bone is an incremental tissue reconciling enamel rhythms, body size, and organismal life history. *Calcified Tissue International*, 84(5), 388-404. https://doi.org/10.1007/s00223-009-9221-2

Bromage, T.G., Juwayeyi, Y.M., Katris, J.A., Gomez, S., Ovsiy, O., Goldstein, J., Janal, M.N., Hu, B., & Schrenk, F. *2016). The scaling of human osteocyte lacuna density with body size and metabolism. *Comptes Rendus Palevol*, 15(1), 32-39. https://doi.org/10.1016/j.crpv.2015.09.001

Canè, V., Marotti, G., Volpi, G., Zaffe, D., Palazzini, S., Remaggi, F., & Muglia, M. A. (1982). Size and density of osteocyte lacunae in different regions of long bones. *Calcified Tissue International*, 34(1), 558-563. https://doi.org/10.1007/BF02411304

Chan, A. H., Crowder, C. M., & Rogers, T. L. (2007). Variation in cortical bone histology within the human femur and its impact on estimating age at death. *American Journal of Physical Anthropology*, 132(1), 80-88. https://doi.org/10.1002/ajpa.20465

Chen, X., Wang, L., Zhao, K., & Wang, H. (2018). Osteocytogenesis: roles of physicochemical factors, collagen cleavage, and exogenous molecules. *Tissue Engineering Part B: Reviews*, 24(3), 215-225. https://doi.org/10.1089/ten.teb.2017.0378

Cook, M., Molto, E. L., & Anderson, C. (1988). Possible case of hyperparathyroidism in a Roman period skeleton from the Dakhleh Oasis, Egypt, diagnosed using bone histomorphometry. *American Journal of Physical Anthropology*, 75(1), 23-30. https://doi.org/10.1002/ajpa.1330750104

Crowder, C., & Stout, S. (Eds.). (2011). *Bone Histology: An Anthropological Perspective*. Boca Raton: CRC Press.

Crowder, C., Dominguez, V. M., Heinrich, J., Pinto, D., & Mavroudas, S. (2022). Analysis of histomorphometric variables: Proposal and validation of osteon definitions. *Journal of Forensic Sciences*, 67(1), 80-91. https://doi.org/10.1111/1556-4029.14949

Cruz, L., Buldyrev, S. V., Peng, S., Roe, D. L., Urbanc, B., Stanley, H. E., & Rosene, D. L. (2005). A statistically based density map method for identification and quantification of regional differences in microcolumnarity in the monkey brain. *Journal of Neuroscience Methods*, 141(2), 321-332. https://doi.org/10.1016/j.jneumeth.2004.09.005

de Buffrénil, V., de Ricqlès, A. J., Zylberberg, L., & Padian, K. (Eds.). (2021). *Vertebrate Skeletal Histology and Paleohistology*. CRC Press.

Dempster, D.W., Compston, J.E., Drezner, M.K., Glorieux, F.H., Kanis, J.A., Malluche, H., Meunier, P.J., Ott, S.M., Recker, R.R., & Parfitt, A.M. (2013). Standardized nomenclature, symbols, and units for bone histomorphometry: a 2012 update of the report of the ASBMR Histomorphometry Nomenclature Committee. *Journal of Bone and Mineral Research*, 28(1), 2-17. https://doi.org/.10.1002/jbmr.1805

Drew, E. R., Mahoney, P., & Miszkiewicz, J. J. (2021). Osteocyte lacuno-canalicular microstructure across the mid-shaft femur in adult males from medieval England. *International Journal of Osteoarchaeology*, 31(2), 176-187. https://doi.org/10.1002/oa.2937

Erben R.G., & Glösmann M. (2019). Histomorphometry in rodents. In A. Idris A. (Ed.) *Bone Research Protocols*. *Methods in Molecular Biology*, *vol 1914* (pp. 411-435). New York, NY: Humana Press, https://doi.org/10.1007/978-1-4939-8997-3_24

Fernández, C., Lysakowski, A. N. N. A., & Goldberg, J. M. (1995). Hair-cell counts and afferent innervation patterns in the cristae ampullares of the squirrel monkey with a comparison to the chinchilla. *Journal of Neurophysiology*, 73(3), 1253-1269. https://doi.org/10.1152/jn.1995.73.3.1253

Frost, H. M. (1987). Secondary osteon population densities: an algorithm for estimating the missing osteons. *American Journal of Physical Anthropology*, 30(S8), 239-254. https://doi.org/10.1002/ajpa.1330300513

Gocha, T. P., & Agnew, A. M. (2016). Spatial variation in osteon population density at the human femoral midshaft: histomorphometric adaptations to habitual load environment. *Journal of Anatomy*, 228(5), 733-745. https://doi.org/10.1111/joa.12433

Gorelik, R., & Gautreau, A. (2014). Quantitative and unbiased analysis of directional persistence in cell migration. *Nature Protocols*, 9(8), 1931-1943. https://doi.org/10.1038/nprot.2014.131

Hunter, R. L., & Agnew, A. M. (2016). Intraskeletal variation in human cortical osteocyte lacunar density: implications for bone quality assessment. *Bone Reports*, 5, 252-261. https://doi.org/10.1016/j.bonr.2016.09.002

Kollmannsberger, P., Kerschnitzki, M., Repp, F., Wagermaier, W., Weinkamer, R., & Fratzl, P. (2017). The small world of osteocytes: connectomics of the lacuno-canalicular network in bone. *New Journal of Physics*, 19(7), 073019. https://doi.org/10.1088/1367-2630/aa764b

Lassen, N.E., Andersen, T.L., Pløen, G.G., Søe, K., Hauge, E.M., Harving, S., Eschen, G.E.T. and Delaisse, J.M. (2017). Coupling of bone resorption and formation in real time: new knowledge gained from human Haversian BMUs. *Journal of Bone and Mineral Research*, 32(7), 1395-1405. https://doi.org/10.1002/jbmr.3091

Maggiano, I. S., Maggiano, C. M., Clement, J. G., Thomas, C. D. L., Carter, Y., & Cooper, D. M. (2016). Three-dimensional reconstruction of Haversian systems in human cortical bone using synchrotron radiation-based micro-CT: morphology and quantification of branching and transverse connections across age. *Journal of Anatomy*, 228(5), 719-732. https://doi.org/10.1111/joa.12430

Martin, R. B. (2007). Targeted bone remodeling involves BMU steering as well as activation. *Bone*, 40(6), 1574-1580. https://doi.org/10.1016/j.bone.2007.02.023

Miszkiewicz, J. J. (2014). Ancient human bone histology and behaviour. PhD Thesis, University of Kent.

Miszkiewicz, J. J. (2015). Histology of a Harris line in a human distal tibia. *Journal of Bone and Mineral Metabolism*, 33(4), 462-466. https://doi.org/10.1007/s00774-014-0644-0

Miszkiewicz, J. (2020). The importance of open access software in the analysis of bone histology in biological anthropology. *Evolutionary Anthropology* 29(4), 165-167 https://doi.org/10.1002/evan.21859

Miszkiewicz, J. J., & Mahoney, P. (2012). Bone microstructure and behaviour in "gracile" and "robust" adult males from the Medieval Period, Canterbury, UK. *American Journal of Physical Anthropology*, 147(54), 215-216.

Miszkiewicz, J.J., Rider, C., Kealy, S., Vrahnas, C., Sims, N.A., Vongsvivut, J., Tobin, M.J., Bolunia, M.J.L.A., De Leon, A.S., Peñalosa, A.L. and Pagulayan, P.S., 2020. Asymmetric midshaft femur remodeling in an adult male with left sided hip joint ankylosis, Metal Period Nagsabaran, Philippines. *International Journal of Paleopathology*, 31, 14-22. https://doi.org/10.1016/j.ijpp.2020.07.003

O'Driscoll, S. W., Marx, R. G., Fitzsimmons, J. S., & Beaton, D. E. (1999). Method for automated cartilage histomorphometry. *Tissue Engineering*, 5(1), 13-23. https://doi.org/10.1089/ten.1999.5.13

Paine, R. R., & Brenton, B. P. (2006). Dietary health does affect histological age assessment: an evaluation of the Stout and Paine (1992) age estimation equation using secondary osteons from the rib. *Journal of Forensic Sciences*, 51(3), 489-492. https://doi.org/10.1111/j.1556-4029.2006.00118.x

Revell, P. A. (1983). Histomorphometry of bone. *Journal of Clinical Pathology*, 36(12), 1323-1331. http://dx.doi.org/10.1136/jcp.36.12.1323

Rose, D. C., Agnew, A. M., Gocha, T. P., Stout, S. D., & Field, J. S. (2012). The use of geographical information systems software for the spatial analysis of bone microstructure. *American Journal of Physical Anthropology*, 148(4), 648-654. https://doi.org/10.1002/ajpa.22099

Sawada, J., Kondo, O., Nara, T., Dodo, Y., & Akazawa, T. (2004). Bone histomorphology of the Dederiyeh Neanderthal child. *Anthropological Science*, 112(3), 247-256. https://doi.org/10.1537/ase.00094

Schindelin, J., Rueden, C. T., Hiner, M. C., & Eliceiri, K. W. (2015). The ImageJ ecosystem: An open platform for biomedical image analysis. *Molecular Reproduction and Development*, 82(7), 518-529. https://doi.org/10.1002/mrd.22489

Sims, N. A., & Martin, T. J. (2014). Coupling the activities of bone formation and resorption: a multitude of signals within the basic multicellular unit. *BoneKEy Reports*, 3. https://doi.org/10.1038/bonekey.2013.215

Smit, T. H., Burger, E. H., & Huyghe, J. M. (2002). A case for strain-induced fluid flow as a regulator of BMU-coupling and osteonal alignment. *Journal of Bone and Mineral Research*, 17(11), 2021-2029. https://doi.org/10.1359/jbmr.2002.17.11.2021

Stout, S. D., & Stanley, S. C. (1991). Percent osteonal bone versus osteon counts: the variable of choice for estimating age at death. *American Journal of Physical Anthropology*, 86(4), 515-519. https://doi.org/10.1002/ajpa.1330860407

Stout, S. D., & Crowder, C. (2012). Bone remodeling, histomorphology, and histomorphometry. In C. Crowder & S. D. Stout (Eds.) *Bone Histology: An Anthropological Perspective* (pp. 1-22). Boca Raton: CRC Press.

Stout, S. D., & Lueck, R. (1995). Bone remodeling rates and skeletal maturation in three archaeoloqical skeletal populations. *American Journal of Physical Anthropology*, 98(2), 161-171. https://doi.org/10.1002/ajpa.1330980206

Stout, S. D., Cole, M. E., & Agnew, A. M. (2019). Histomorphology: Deciphering the metabolic record. In J. E. Buikstra (Ed.) *Ortner's Identification of Pathological Conditions in Human Skeletal Remains* (pp. 91-167). Elsevier Academic Press.

Sugawara, Y., Kamioka, H., Honjo, T., Tezuka, K. I., & Takano-Yamamoto, T. (2005). Three-dimensional reconstruction of chick calvarial osteocytes and their cell processes using confocal microscopy. *Bone*, 36(5), 877-883. https://doi.org/10.1016/j.bone.2004.10.008

Wang, L., Cowin, S. C., Weinbaum, S., & Fritton, S. P. (2000). Modeling tracer transport in an osteon under cyclic loading. *Annals of Biomedical Engineering*, 28(10), 1200-1209. https://doi.org/10.1114/1.1317531

Wang, M., Han, X., Liu, C., Takayama, R., Yasugi, T., Ei, S.I., Nagayama, M., Tanaka, Y. and Sato, M., 2021. Intracellular trafficking of Notch orchestrates temporal dynamics of Notch activity in the fly brain. *Nature Communications*, 12(1), 1-15. https://doi.org/10.1038/s41467-021-22442-3

van Tol, A.F., Roschger, A., Repp, F., Chen, J., Roschger, P., Berzlanovich, A., Gruber, G.M., Fratzl, P. and Weinkamer, R., 2020. Network architecture strongly influences the fluid flow pattern through the lacunocanalicular network in human osteons. *Biomechanics and Modeling in Mechanobiology*, 19(3), 823-840. https://doi.org/10.1007/s10237-019-01250-1

Villa, C., & Lynnerup, N. (2010). A stereological analysis of the cross-sectional variability of the femoral osteon population. *American Journal of Physical Anthropology*, 142(3), 491-496. https://doi.org/10.1002/ajpa.21269